

1 **Adaptive COF-PVDF Composite Artificial Solid Electrolyte Interphase for Stable Aqueous Zinc Batteries**

2

3 Vipada Aupama¹, Jinnawat Sangsawang¹, Wathanyu Kao-ian¹, Suttipong Wannapaiboon², Jirapha Pimoei¹,

4 Warunyoo yoopensuk¹, Montree Opchoei¹, Zari Tehrani³, Serena Margadonna³, Soorathep Kheawhom^{1,4,*}

5

6 ¹ Department of Chemical Engineering, Faculty of Engineering, Chulalongkorn University, Bangkok
7 10330, Thailand

8 ² Synchrotron Light Research Institute, 111 University Avenue, Muang District, Nakhon Ratchasima
9 30000, Thailand

10 ³ Department of Chemical Engineering, Faculty of Engineering, Swansea University, Swansea SA1 8EN,
11 United Kingdom

12 ⁴ Center of Excellence on Advanced Materials for Energy Storage, Chulalongkorn University, Bangkok
13 10330, Thailand

14

15 **Corresponding author: soorathep.k@chula.ac.th*

16

17

18

19 **Abstract**

20 The cyclability of aqueous zinc (Zn) – based batteries is limited by the formation of dendrites and side
21 reactions. Herein, this work presents a composite- artificial solid electrolyte interphase (ASEI) in two
22 stages. Firstly, a covalent organic framework (COF) is synthesized via an interfacial reaction between
23 aldehyde and amine linkers. Secondly, polyvinylidene fluoride (PVDF) is additionally coated on top of the
24 COF film via spin coating. Results demonstrate that the COF-PVDF composite regulates Zn ion flux,
25 preventing dendrite formation and reducing side reactions, while dynamically adapting to large volume
26 changes. Zn plating/stripping tests with a symmetrical cell reveal that PVDF@COF@Zn exhibits enhanced
27 stability and higher coulombic efficiency (CE) compared to bare Zn. Furthermore, the full cell incorporating
28 PVDF@COFs@Zn//I₂@C signifies significantly enhanced stability, making PVDF@COFs a promising
29 ASEI material for stable aqueous Zn batteries. It is crucial to emphasize that the chemical and mechanical
30 properties are the key parameters in designing the ASEI, as these factors directly influence its performance
31 and longevity.

32 **Keywords:** Aqueous Zinc Batteries; Artificial Solid Electrolyte Interphase; Covalent Organic Framework;
33 Polyvinylidene Fluoride; Dendrite Suppression

34

35 **1. Introduction**

36 Of late, the growing demand for energy and rising environmental concerns have necessitated the
37 development of reliable electrical energy storage (EES) systems to harness renewable resources [1-7]
38 Among various rechargeable battery technologies, lithium-ion batteries (LIBs) are the most successful,
39 offering high energy density and long cycle life. They have been used in portable electronics, electric
40 vehicles, and grid storage. However, LIBs still face significant challenges that consequently impact their
41 sustainability and scalability [8, 9].

42 A major challenge in LIBs is the use of flammable and toxic organic electrolytes, posing safety
43 risks under high-stress conditions like overcharging or short-circuiting [10]. This has led to incidents of
44 battery fires and explosions, highlighting the need for safer alternatives [2]. Additionally, LIBs are costly
45 due to the use of expensive materials like lithium, cobalt, and nickel, which makes large-scale deployment
46 challenging, particularly for grid storage.

47 Environmental issues also arise from the extraction, processing, and disposal of LIB materials [11,
48 12]. The mining of lithium and cobalt, for instance, is associated with significant environmental degradation
49 and social impacts, including habitat destruction, water pollution, and human rights violations [13]. The

50 limited availability of these materials further exacerbates supply chain vulnerabilities and raises concerns
51 about the long-term sustainability of LIB technology. In light of these challenges, researchers are exploring
52 alternative energy storage solutions that offer improved safety, cost-effectiveness, and environmental
53 sustainability [14]. Among these alternatives, rechargeable zinc-based batteries, particularly aqueous Zn-
54 ion batteries (AZIBs), have shown such a great promise as future candidates for large-scale energy storage
55 applications [15, 16]. AZIBs offer several advantages over LIBs, including the use of non-toxic and
56 abundant materials plus inherent safety due to aqueous electrolytes, and economical feasibility.

57 Due to their cost-effectiveness, high theoretical specific capacity, low redox potential, and natural
58 abundance [17]. However, several issues, such as hydrogen evolution reaction (HER), Zn corrosion,
59 passivation, and dendritic Zn formation, plague ZMAs, reducing CE and battery lifespan [18, 19]. To
60 address these issues and improve the performance and stability of ZMAs, various strategies have been
61 developed [20, 21]. One approach involves enhancing electrolytes by adding inorganic or organic molecules
62 as additives. These additives can help suppress side reactions and improve the uniformity of Zn deposition
63 [19]. This strategy, however, often increases the viscosity of the electrolytes, which may affect ionic
64 diffusion and overall battery performance. Moreover, some novel additives are costly, limiting their
65 practical application [22].

66 A particularly promising strategy is the development of artificial solid electrolyte interphases
67 (ASEIs) as protective layers. ASEIs can be engineered to provide both chemical and mechanical protection
68 to the Zn anode, thereby enhancing its performance and stability [21, 23]. Most ASEIs are designed
69 considering their chemical-functional properties. For instance, layered double hydroxides (LDHs)-based
70 materials, such as PA6/Zn(TfO)₂/LDH and Mg-Al LDH, consist of charged layers and interlayer anions
71 that enhance Zn²⁺ transport [23-27]. Organic polymers like polyamide (PA), polyacrylonitrile (PAN), and
72 poly(vinyl butyral) (PVB) possess unique bonding networks and a strong ability to coordinate with Zn²⁺,
73 helping suppress side reactions and promote uniform Zn deposition [28-30]. Metal-organic frameworks
74 (MOFs), especially zeolitic imidazolate frameworks (ZIF-7, ZIF-8, ZIF-11), control Zn²⁺ diffusion,
75 nucleation, and deposition by promoting ion flux on Zn metal anodes and blocking electrons with their
76 porous insulating structures [31-33]. Yet, the modification of MOFs is often hindered by cost and
77 complexity [34].

78 Covalent organic frameworks (COFs) have emerged as versatile alternatives for creating ASEIs.
79 COFs are crystalline porous polymers constructed from organic building blocks through strong covalent
80 bonds [35, 36]. These frameworks can be synthesized through various methods, including traditional
81 solvothermal techniques and simpler room-temperature synthesis methods, such as solution synthesis [34],

82 interfacial-reaction methods [37], and Schiff base reaction (involving amines and aldehydes) [38]. For
83 example, Grzybowski et al. [37] developed nanoporous COF films that suppress dendrite growth and the
84 formation of electrochemically inactive Zn byproducts, promoting uniform Zn deposition. Recently, a
85 sulfonic acid-containing COF (TpPa-SO₃H) has been applied to boost the conductivity and protective
86 qualities of Zn anodes [37]. Moreover, COFs consist of ketone (C=O) and imine (N-H) functional groups,
87 offering nucleophilic sites that transiently interact with Zn²⁺, promoting a more homogeneous flow of Zn²⁺
88 through the COF layer, thereby facilitating even Zn nucleation and deposition [34, 39, 40].

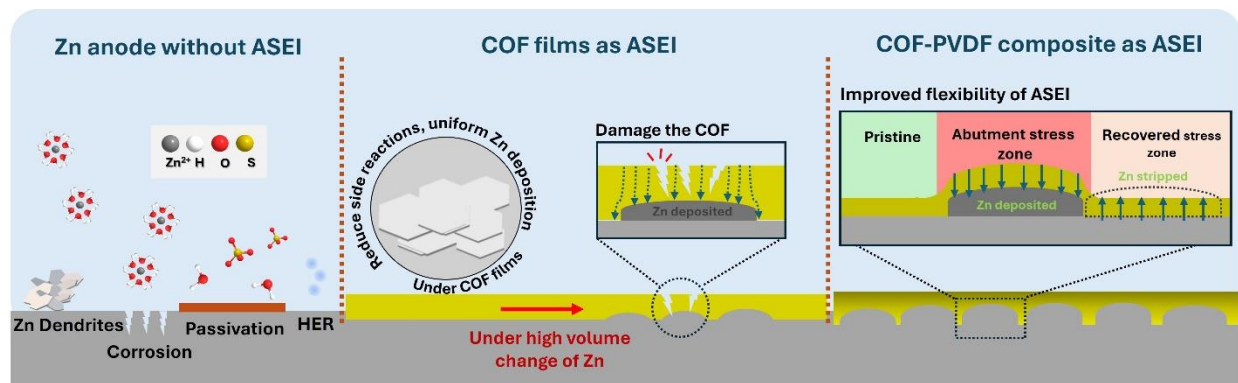
89 Despite their promising features, COFs face challenges related to their mechanical properties.
90 During charging and discharging processes, significant volume changes in the Zn anode damage the ASEI
91 layers. Ideally, the protective layer can accommodate these mechanical properties [20, 41]. It is noted that
92 a high-quality dynamic interface will buffer surface changes, maintaining constant contact with the
93 electrode during volume changes. The design of the ASEI layer is significant and vital, requiring
94 optimization of both chemical and mechanical properties to improve long-term performance and
95 adaptability under various conditions such as high capacity. To achieve this ideal, a modified composite
96 ASEI was developed from a COF structure rich in functional groups capable of interacting with Zn²⁺
97 without significantly affecting the resistance in the battery. The polymer matrix acts as a framework
98 covering the COF layer, providing flexibility which can adaptive during the volume changes of Zn
99 deposition due to the plating/stripping process.

100 In this work, we propose a modified ASEI layer developed from a COF-PVDF composite. The
101 COF film, synthesized from aldehyde and amine linkers, contains C=O and N-H moieties that promote
102 uniform Zn²⁺ deposition and inhibit Zn dendrite growth, while also decreasing nucleation overpotential and
103 suppressing side reactions through interactions with Zn²⁺ [21, 39, 40]. The PVDF solution was spin-coated
104 onto the COF layer, where the β-PVDF form interacts with the COF through non-covalent interactions
105 (NH----F & C=O----CH) in β-PVDF and the C=O group in the COF. This interaction creates a new surface
106 morphology, enhancing the ASEI layer's effectiveness, particularly under high-stress conditions. Besides,
107 the β-PVDF form exhibits high polarity (ferroelectric properties), facilitating the transfer of Zn²⁺ ions
108 through the COF layer more easily [42].

109 The synthesis method involves an interfacial reaction technique designed to improve the COF
110 layer's stability during cycling. An amine solution is introduced onto an aldehyde solution at a water-oil
111 interface containing COFs, after which the COF films are transferred to the surface of the Zn anode as an
112 ASEI layer. The PVDF solution is then cast on top of the COF layer via spin coating, followed by heat
113 treatment at 60°C in a closed system. This process yields the β-PVDF type, which enhances flexibility and

114 promotes Zn^{2+} transfer through the ASEI layer due to its higher polarity compared to other forms of PVDF
115 [43]. The composite ASEI offers a promising approach to enhancing the stability and performance of Zn-
116 based batteries, as depicted in **Fig. 1**.

117



118

119 **Figure 1.** Schematic diagram of the issues that occur during the stripping/plating process and the
120 configuration of the COF-PVDF as ASEI.

121 2. Materials and methods

122 2.1 Materials

123 All chemicals and materials used in this study were commercially available and employed without any
124 further purification. 2,4,6-Triformylphloroglucinol (Tp, >98.0%, GC, TCI) was used as the aldehyde
125 monomer, and 4,4'-Diaminobenzophenone (Bp, >98.0%, T, HPLC, TCI) was used as the amine monomer.
126 As a solvent for the amine monomer, p-Toluenesulfonic acid (PTSA, >98.0%, TCI) was used.
127 Dichloromethane (DCM, >99.5%, Ajax Finechem) was used as a solvent for the aldehyde monomer.
128 Dimethylacetamide (DMAc, >99.5%, Honeywell) and acetone were used as solvent and for washing the
129 obtained COF films. Polyvinylidene fluoride (PVDF, MW 275000, GPC, ALDRICH) was used as the
130 polymer matrix. Zn sulfate heptahydrate ($ZnSO_4 \cdot 7H_2O$, $\geq 99.0\%$, Kemaus) was used as the metal salt for
131 the battery electrolyte. Zn foil (thickness 0.1 mm) and copper foil (thickness 0.05 mm) were used as
132 substrates.

133

134 **2.2 Methods**

135 **2.2.1 Preparation of the COF film**

136 The COF film was synthesized via an interfacial reaction between two liquid phases. Initially, 14 mg (0.067
137 mmol) of 2,4,6-Triformylphloroglucinol (Tp) was dissolved in 50 ml of dichloromethane. This aldehyde
138 solution was then poured into a beaker, and deionized (DI) water was carefully added on top to create a
139 spacer layer. Subsequently, 25 mg (0.117 mmol) of 4,4'-Diaminobenzophenone (Bp) and 54 mg (0.313
140 mmol) of p-Toluenesulfonic acid (PTSA) were dissolved in 50 ml of DI water, and this solution was slowly
141 added on top of the spacer water. The reaction was maintained at room temperature for 72 h under stable
142 conditions (**Fig. S1**). Next, the COF films formed at the interface were collected by carefully removing the
143 top solution. Then, the films were thoroughly washed with water, dimethylacetamide (DMA), and acetone.
144 Finally, the COF films were transferred to the Zn anode. Typically, the thickness of the COF films depends
145 on the reaction time. In this work, maintaining the reaction for 72 h resulted in films with a thickness of ~
146 200-300 nm, as observed in the cross-section with FE-SEM (**Fig. S2**).

147 **2.2.2 Preparation of the COF-PVDF films as ASEI**

148 After coating the COF films, a 10 wt% PVDF solution was prepared by dissolving PVDF in
149 dimethylacetamide (DMA) and carefully dropped onto the COF film. Spin coating was used to spread the
150 PVDF solution uniformly. Subsequently, the samples were placed on a hotplate at 60°C for 90 min to
151 evaporate the solvent slowly in an enclosed system, ensuring a stable and well-adhered PVDF layer on the
152 COF films.

153 **2.2.3 Preparation of I₂@C as cathode material**

154 Solid iodine and activated carbon were thoroughly mixed in a 2:3 weight ratio using a mortar. The mixture
155 was then placed in a sealed glass tube, which was heated at 80°C for 4 h in a vacuum oven. To prepare the
156 cathode electrode, the I₂-activated carbon composite (I₂@C) was used as the cathode material. For the
157 cathode electrode preparation, the I₂@C composite was combined with Super P and CMC binder in an 8:1:1
158 weight ratio using DI water as the solvent. The mixture was stirred at 300 rpm at room temperature until it
159 became homogeneous. The resulting slurry was coated onto a graphite foil current collector and dried at
160 room temperature [44, 45].

161 **2.2.4 Preparation of battery cells for electrochemical tests**

162 Herein, the CR2025-coin cells were assembled, and tested in three configurations. In the symmetrical cells,
163 both sides of the electrode used Zn foil with COF-coated and COF-PVDF composite layers; bare Zn was
164 used for comparison with the ASEI layer. For the asymmetrical cells, the anode was copper foil-coated with

165 the ASEI layer. In contrast, the electrode was Zn foil-coated. In the full-cell configuration, the cathode was
166 composed of I₂@C, and the anode was Zn metal with a different ASEI layer. In all configurations, a GF/A
167 filter (Whatman®) was used as the separator, while the electrolyte was 2 M ZnSO₄ (an aqueous solution).

168 2.3 Characterization and measurement

169 2.3.1 Chemical and structural characterization

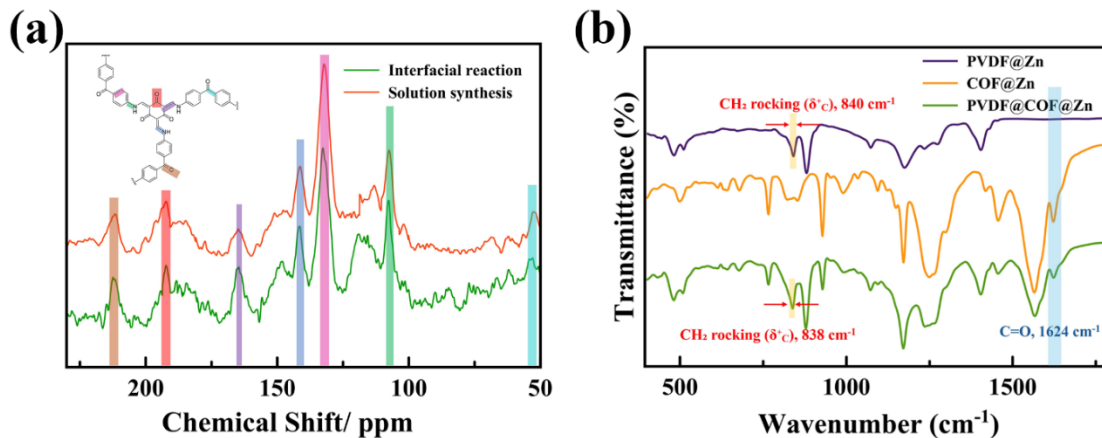
170 To verify the structure of the COFs, both a 400 MHz Fourier transform nuclear magnetic resonance (NMR)
171 spectrometer (solid-state NMR, BRUKER AVANCE III HD/Ascend 400 WB, Bruker, USA) and a Fourier
172 transform infrared (FT-IR) spectrometer (Perkin Elmer Spectrum One, USA) were employed. The surface
173 morphology of the samples was examined, using field emission scanning electron microscope (FE-SEM,
174 Quanta-250 FEG, FEI, USA). X-ray diffraction (XRD) in grazing incidence mode using monochromatic
175 X-ray with an energy of 12 keV was performed at the Beamline BL1.1W (Synchrotron Light Research
176 Institute, Thailand) to determine the crystalline phase formation and crystal structure of the ASEI coated
177 on the Zn electrodes and to investigate the side reactions occurred on the Zn anode after cycling process.

178 2.3.2 Electrochemical measurement

179 To conduct galvanostatic charge-discharge (GCD) measurements, both symmetrical and asymmetrical cells
180 were tested using battery tester (CT-4008-5V20mA; Neware Technology, China). The electrochemical
181 properties were further assessed using cyclic voltammetry (CV) and electrochemical impedance
182 spectroscopy (EIS) with Squidstat Plus (Admiral Instruments, USA).

183 3. Results and discussion

184 3.1 Characterization of protective layers

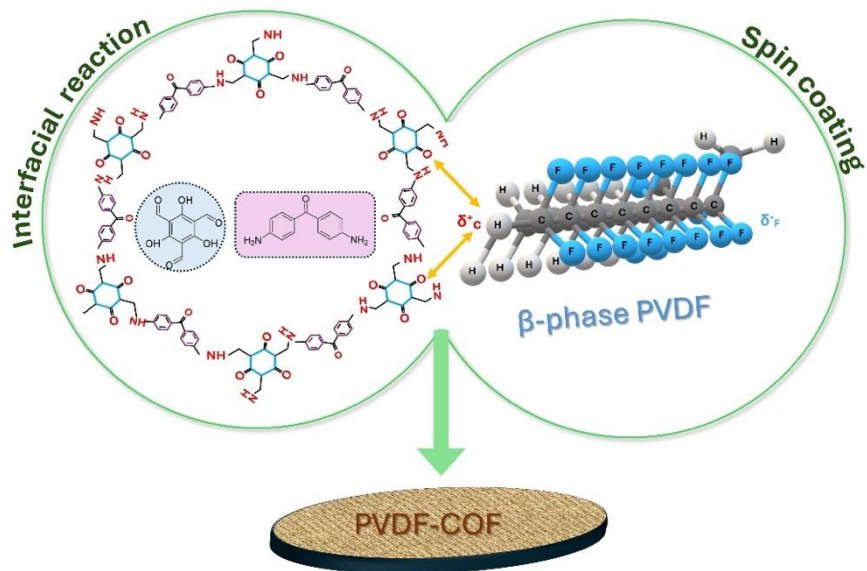


185
186 **Figure 2.** Schema of the COFs and PVDF structure: (a) The ¹³C CP-MAS solid-state NMR spectra of COF
187 film obtained with different methods, and (b) The FTIR spectra of COF, PVDF, and COF-PVDF structures.

188 In **Fig.2**, the structure of the COF layer is illustrated by correlation with the ^{13}C CP-MAS solid-state NMR
189 spectra. The spectra exhibit peaks at 183 ppm, 145 ppm, and 120 ppm, corresponding to the carbonyl carbon
190 ($\text{C}=\text{O}$), enamine carbon ($=\text{C}-\text{NH}$), and α -enamine carbon in keto form, respectively [34, 39, 40]. These
191 findings also confirm the formation of an imine group. It is evident that the COF structure synthesized via
192 the interfacial reaction has an identical ^{13}C CP-MAS peak pattern to the COF structure synthesized via the
193 dip coating, as previously reported by Aupama et al., [40]. These COF structures, featuring $\text{C}=\text{O}$ and $\text{N}-\text{H}$
194 functional groups, can interact with Zn^{2+} ions. Moreover, this interfacial reaction can produce uniform COF
195 films capable of coating the Zn anode, as illustrated in **Fig. S3**. This single protective layer is denoted as
196 COF@Zn.

197 Subsequently, a PVDF polymer was coated on top of COF@Zn, forming the ASEI layer denoted
198 as PVDF@COF@Zn. The sample was then heated to 60°C , inducing the transformation of the PVDF
199 polymer to its β -phase. The β -PVDF structure was confirmed via its FTIR spectrum, which shows peaks at
200 510 cm^{-1} (CF_2 bending) and 840 cm^{-1} (CH_2 rocking), affirming the presence of the β -phase of PVDF in
201 PVDF@COF@Zn [43, 46]. The β -PVDF structure interacts with COF structures through the attraction
202 between the partially positively charged carbon atoms in β -PVDF ($\delta^+\text{C}-\text{C}=\text{O}$) and the partially negative-
203 charged carbonyl group ($\text{C}=\text{O}$) in the COF structure [46]. FTIR results confirm this interaction, as observed
204 by the shift of the CH_2 rocking mode (typically at 840 cm^{-1}) to a lower wavenumber (838 cm^{-1}). Normally,
205 $\text{C}=\text{O}$ stretches occur between $1650\text{-}1750\text{ cm}^{-1}$, but significant electronic effects from π - π stacking (**Fig. S4**)
206 can shift these stretches to a lower frequency e.g. 1624 cm^{-1} [47, 48]. The reduced intensity of the $\text{C}=\text{O}$
207 peak at 1624 cm^{-1} suggests an interaction between the partially positively charged carbon atoms (CH_2
208 rocking, $\delta^+\text{C}$) and $\text{C}=\text{O}$ groups in the COF structure. This outcome implies that the PVDF layer not only
209 enhances the flexibility of the ASEI layer during substantial volume changes but also promotes Zn^{2+}
210 movement. It is noted that the negatively charged fluoride atoms (CF_2 bending, $\delta^-\text{F}$) in PVDF can easily
211 facilitate the movement of Zn^{2+} through the ASEI structure [43]. In **Fig. 3**, the interaction between the COF
212 structure and β -PVDF is depicted.

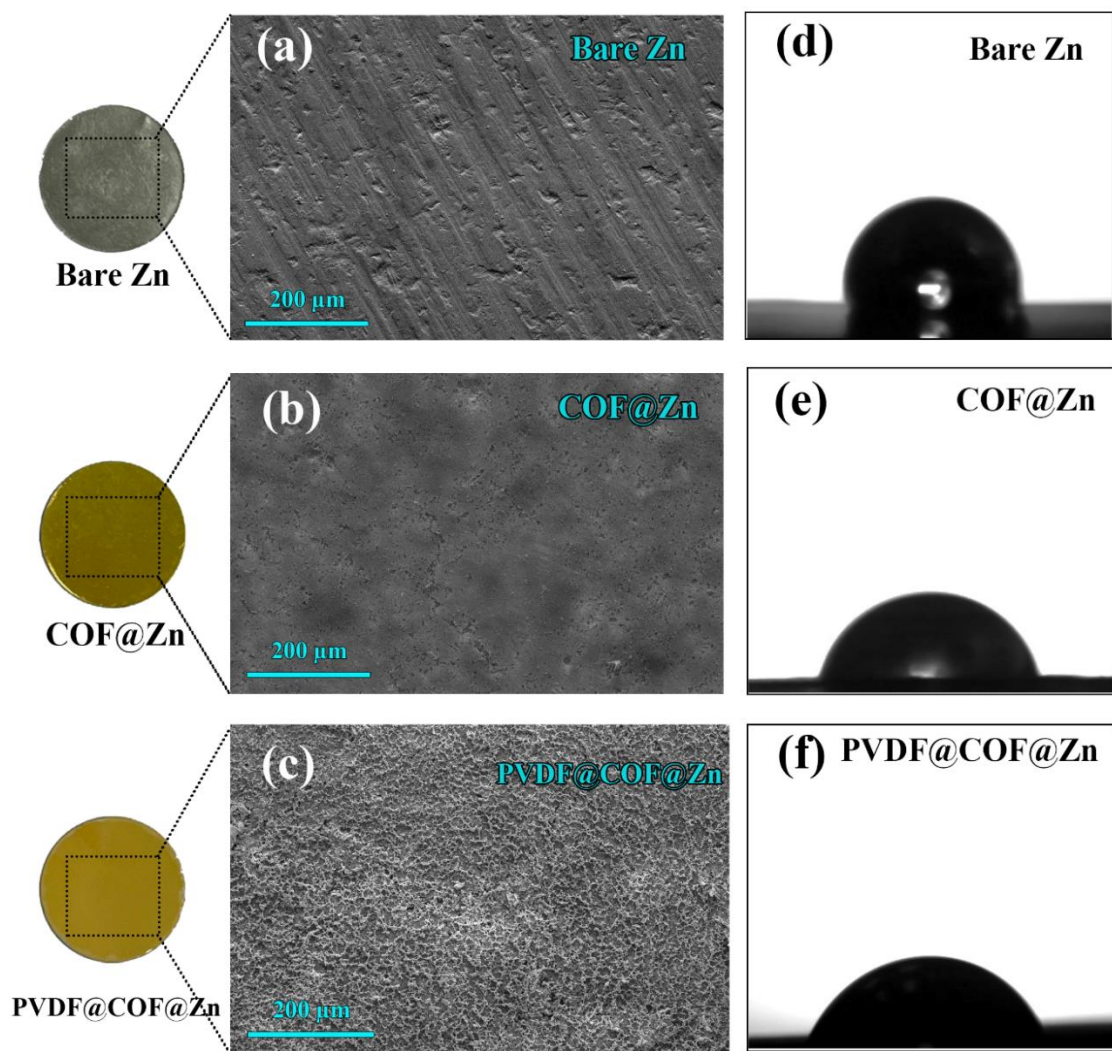
213



214

215 **Figure 3.** Schema illustrating the formation of ASEI from COF and β -PVDF.

216



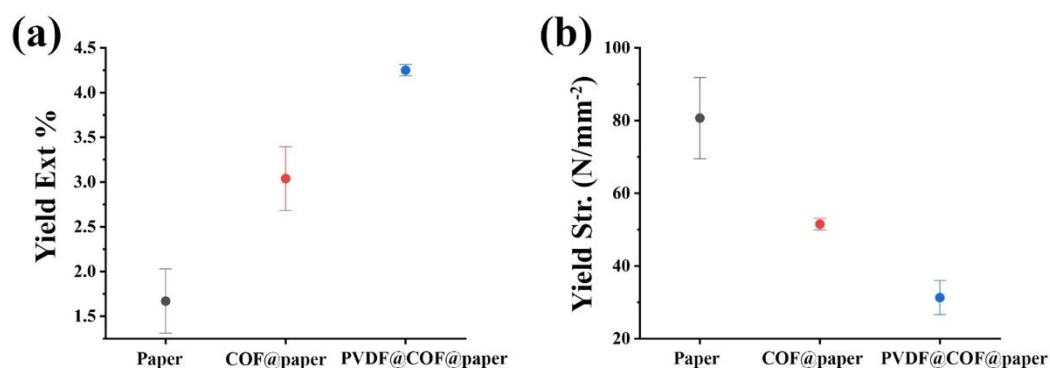
217
 218 **Figure 4.** (a-c) Surface of the different electrodes: Bare Zn, COF@Zn, and PVDF@COF@Zn, and (d-f)
 219 Contact angles for ZnSO₄ droplets on the surface of different Zn anodes: Bare Zn, COF@Zn, and
 220 PVDF@COF@Zn.

221 As shown in **Fig. 4a-c**, the surface morphology of each layer is observed via FE-SEM images. The
 222 PVDF layer forms a continuous coating over the COF layer, acting as a protective shield. This coverage
 223 enhances the mechanical stretching properties of the composite films. During Zn plating/stripping, ASEI
 224 needs to adapt to volume changes and reduce stress, requiring dynamic adaptability. The PVDF composite
 225 increases the elasticity of the ASEI. Although PVDF is a polymer, β -PVDF does not significantly increase
 226 electrode resistance, as confirmed by EIS in **Fig. S5**. Additionally, the negatively charged fluoride side in
 227 PVDF facilitates Zn²⁺ transport [43], improving overall stability and durability without increasing electrode
 228 resistance. Consequently, the PVDF matrix prevents the COF layer from experiencing significant strain due

229 to volume changes in the Zn anode, thereby enhancing the composite's ability to withstand mechanical
230 stress.

231 To assess the zincophilic properties, wettability tests were conducted. Such tests are crucial in
232 designing ASEI or protective layers. These properties greatly influence Zn stripping/plating reaction. Some
233 protective layers can increase Zn^{2+} ion conductivity while others may increase electrode resistance. As
234 shown in **Fig.4d-f**, this behavior was evaluated through contact angle measurements. When Zn salt
235 electrolytes namely $ZnSO_4$ solution were applied to the surface of the anodes, the contact angles for
236 electrodes coated with COF@Zn and PVDF@COF@Zn proved to be smaller compared to those for bare
237 Zn. This outcome indicates enhanced zincophilic properties and improved wettability of the electrodes.

238



239

240 **Figure 5.** Mechanical properties of the ASEI layer: (a) Percent yield extension, and (b) Yield strength.

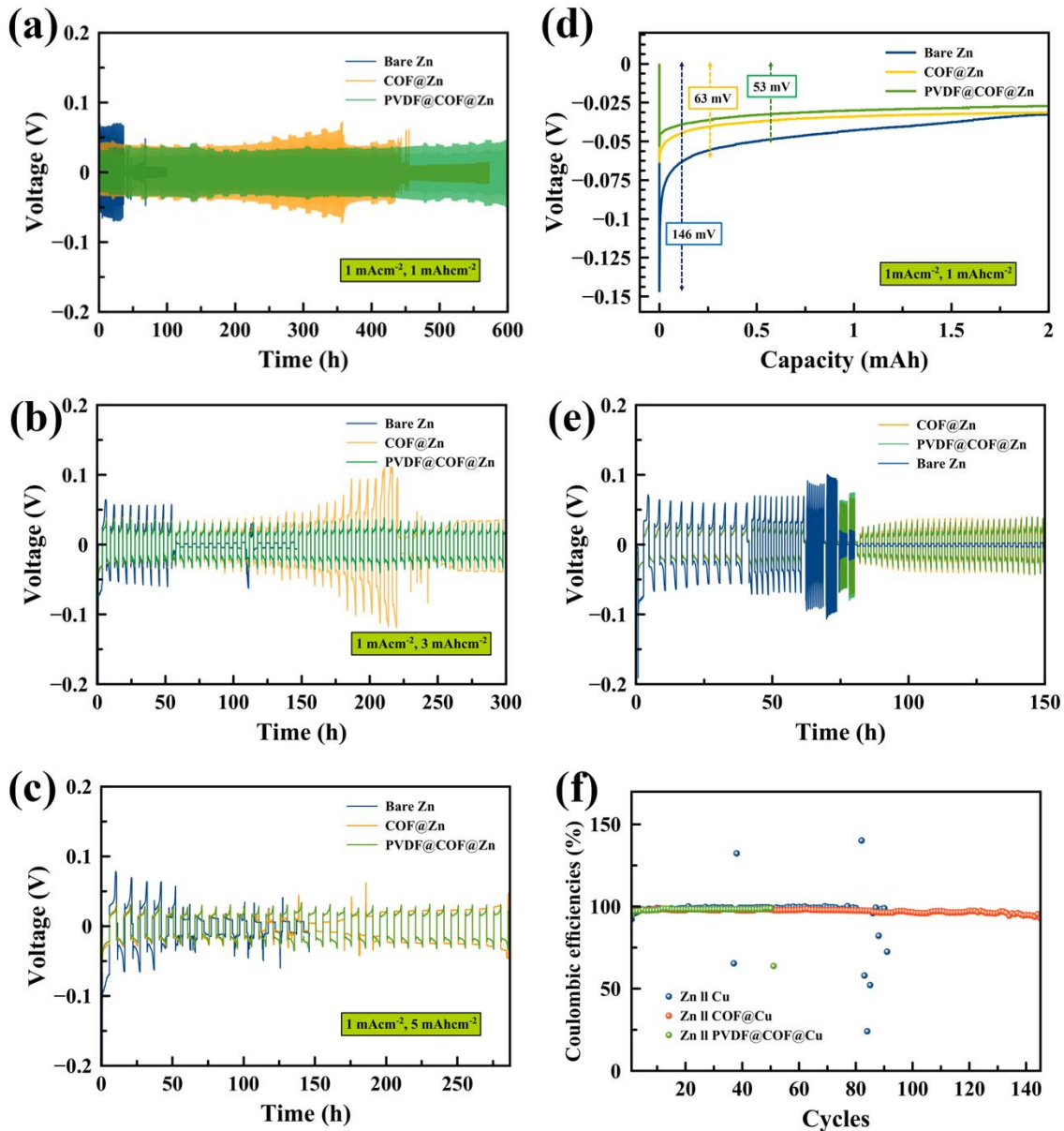
241 The mechanical properties of the ASEI layers were assessed, using a universal testing machine
242 (UTM). The COF layer and PVDF@COF layer were coated on paper for testing. As shown in **Fig. 5a-b**,
243 the percent yield extension of PVDF@COF is higher than that of COF, indicating greater elasticity.
244 Conversely, the yield strength of PVDF@COF is lower than that of COF, which suggests that the addition
245 of PVDF improves the mechanical properties of the ASEI layer. This demonstrates PVDF's effectiveness
246 in enhancing the elasticity of the ASEI layer. These results confirm that the ASEI design from COF-PVDF
247 composite in this study possesses both the functional and mechanical properties necessary for effective
248 performance.

249

250

251 **3.2 Performance of ZIBs in a symmetrical/asymmetrical configuration**

252



253

254 **Figure 6.** Electrochemical performance of symmetrical and asymmetrical cells: (a-c) Long-term GCD
 255 profiles of the bare Zn electrode and Zn electrode coated with ASEI layers at a current density of 1 mA cm^{-2}
 256 and different capacities (1, 2, and 3 mAh cm^{-2}), (d) Voltage profiles of the bare Zn and ASEI-coated Zn
 257 foil during the first plating at a current density of 1 mA cm^{-2} and a capacity of 1 mAh cm^{-2} , (e) Rate
 258 performance of the symmetrical cells at various current densities: 0.5, 1, 2, 3, and 5 mA cm^{-2} , and (f) CE of
 259 the asymmetrical cells.

260 To investigate the improvement of the Zn anode after coating with a COF layer, a symmetrical cell
261 was used in this experiment. In **Fig. 6a**, the stability of Zn stripping/plating on the electrode at a current
262 density of 1 mA cm^{-2} and a capacity of 1 mAh cm^{-2} is shown. It is observed that COF@Zn and
263 PVDF@COF@Zn could operate for longer periods than the bare Zn or cells without any coating layer.

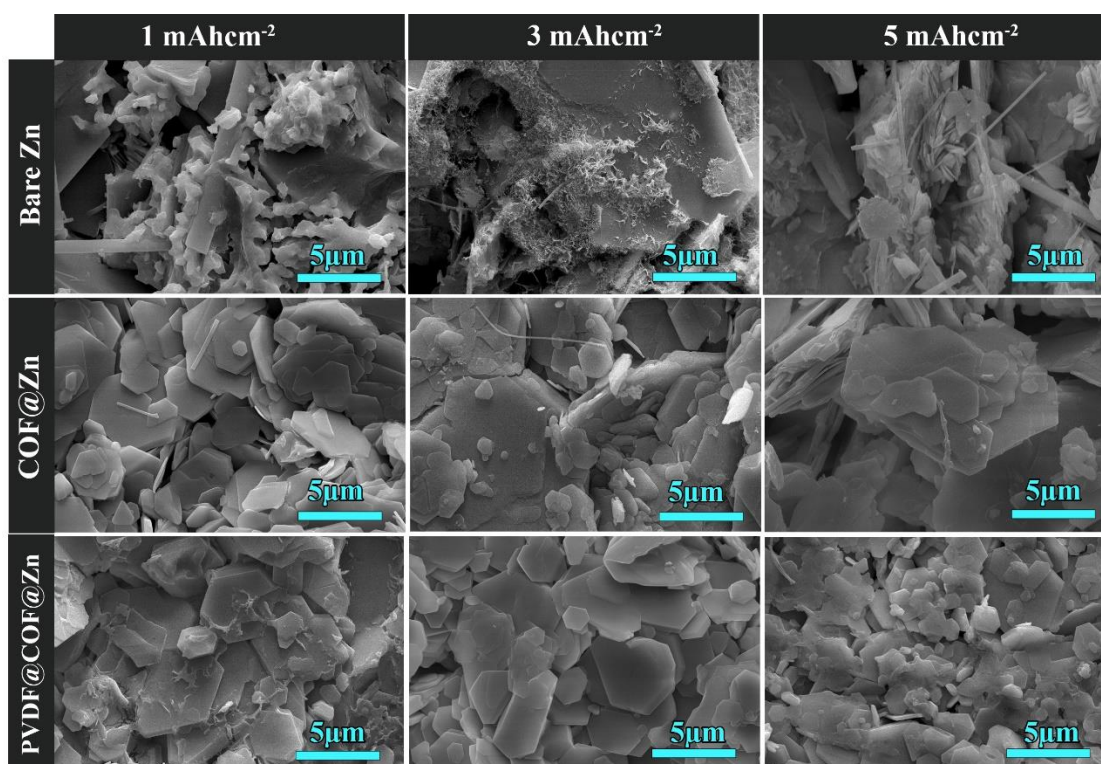
264 This improvement is attributed to the ASEI layer, which ensures uniform Zn deposition. During
265 the deposition process, Zn^{2+} interacts with the C=O and N-H functional groups within the COF structure
266 [40]. Such an effect has a pivotal role in improving the homogeneity of the Zn ion flux, thus ensuring the
267 smooth Zn surface. Moreover, ASEI isolates the Zn metal surface from the electrolyte, which minimizes
268 the side reactions that typically occur on the Zn anode.

269 In **Fig. 6b**, when the charged/discharged capacity increased, the stability of the anode decreased
270 due to significant changes in Zn volume, which increased the chance of Zn cluster formations and Zn
271 dendrites. As the volume of Zn changes, the protective layer must dynamically adapt to surface changes. If
272 the protective layer is not flexible, it cannot absorb the sheer force during volume changes. However,
273 PVDF@COF@Zn was found to operate longer than COF@Zn and bare Zn, indicating better adaptability
274 to changes on the Zn surface. In **Fig. 6c**, it is noted that PVDF@COF@Zn operates longer than COF@Zn
275 under higher Zn volume changes.

276 In **Fig. 6d**, the voltage profile of the first plating at a current density of 1 mA cm^{-2} and a capacity
277 of 1 mAh cm^{-2} is illustrated. The overpotentials of the bare Zn, COF@Zn, and PVDF@COF@Zn were 146
278 mV, 63 mV, and 53 mV, respectively. These findings indicate that the ASEI layer not only increases cycle
279 life performance but also reduces the nucleation overpotential required for Zn deposition. Lower
280 overpotential values for COF@Zn and PVDF@COF@Zn suggest more efficient and stable Zn deposition
281 processes compared to bare Zn.

282 The COF layer serves as a solid Zn ion conductor interface, which accelerates the transfer of Zn^{2+}
283 ions. This layer facilitates the movement of Zn^{2+} by providing pathways that reduce resistance and enhance
284 ion mobility. Additionally, the COF layer enhances the de-solvation of $\text{Zn}(\text{H}_2\text{O})_6^{2+}$ in the bulk electrolyte.
285 De-solvation is the process of removing water molecules attached to the Zn^{2+} ions, which is essential for
286 efficient Zn deposition. By improving the de-solvation process, the COF layer helps in achieving uniform
287 and stable Zn deposition. As confirmed, in **Fig. S4**, XRD results reveal a broader peak around $2\theta = 27^\circ$ that
288 corresponds to π - π stacking between benzene rings in the COF layer, which greatly promotes conductivity.
289 Such stacking induces delocalization and distribution of electrons, resulting in decreased Zn accumulation
290 and improved nucleation of Zn deposition on the anode[34, 40]

291 In **Fig. 6e**, to investigate the effect of current density on the electrode, rate capability experiments
292 were conducted. In **Fig. S6**, it is observed that at various current densities, the stability of the Zn anode
293 coated with the ASEI layer was maintained during current changes, and the morphologies of Zn deposition
294 remained smooth and dense. In particular, the PVDF@COF coating demonstrated stability not only under
295 high volume changes but also at high current densities. It is acknowledged that the reversibility of Zn is an
296 important parameter. In **Fig. 6f**, CE of the different electrodes is compared. As a result, the CE of
297 PVDF@COF@Cu (>99%) was found to be more stable than that of COF@Cu (>98%) and the bare Cu
298 (<96.5%).



299
300 **Figure 7.** Morphologies of Zn on the surface of bare Zn and Zn underneath the COF layer from symmetrical
301 cells after 50 cycles at constant current density 1 mA cm⁻² and various capacities (1, 3, and 5 mAh cm⁻²).

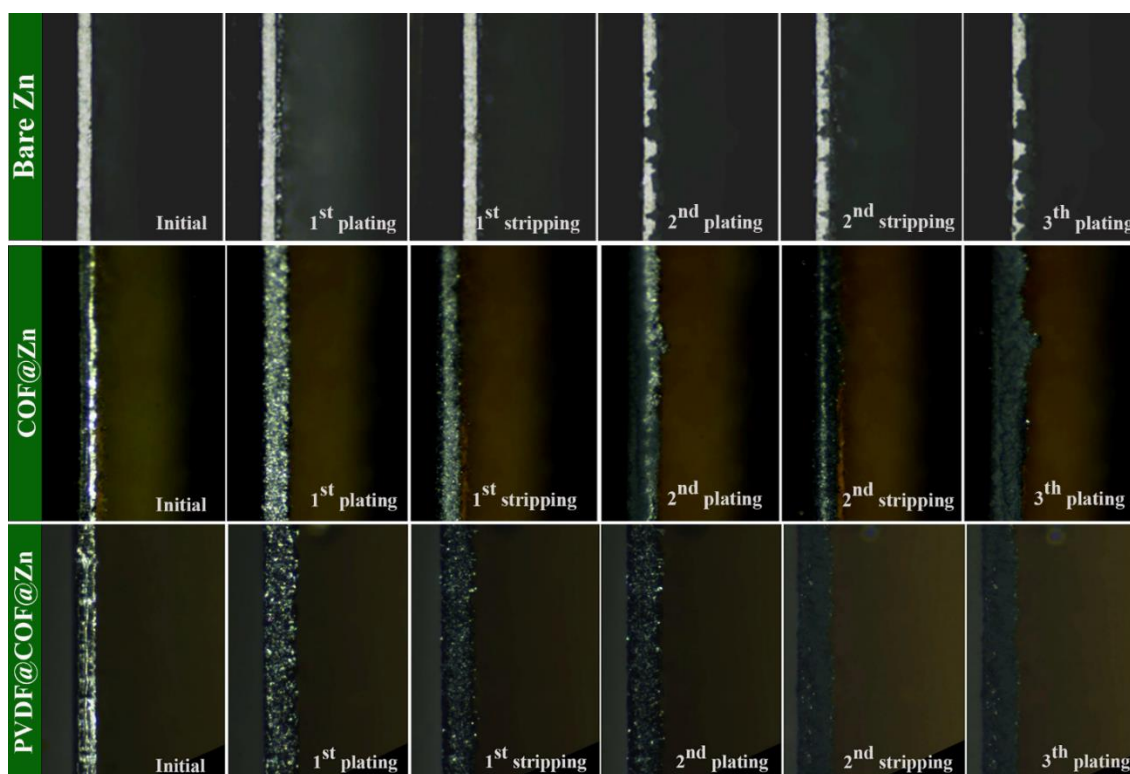
302 In **Fig.7**, after 50 cycles at various capacities in the symmetrical cell, the morphologies of Zn
303 deposition on the surfaces of the bare Zn and Zn underneath the COF layer were analyzed. Results indicate
304 that Zn deposition on bare Zn is inconsistent and non-uniform. In contrast, Zn deposition under COF@Zn
305 and PVDF@COF@Zn layers is seen to be much more uniform, suggesting that these protective layers
306 promote better Zn deposition. However, at 5 mA h cm⁻², the Zn deposits under the single-COF layer were
307 found to be less smooth and flat compared to those under PVDF@COF@Zn. This observation highlights
308 the importance of having a protective layer with mechanical properties that can adapt to the Zn

309 stripping/plating process, ensuring uniform deposition and reducing the risk of dendrite formation. This
310 result also supports the notion that PVDF@COF@Zn has superior adaptive properties compared to
311 COF@Zn alone.

312 In **Figs. S7 and S8**, the GIXRD results show that after 50 and 100 cycles, respectively, the
313 diffraction peaks at 8.068° correspond to the zinc hydroxide sulfate (ZHS) phase. Thus, the bare Zn exhibits
314 a sharper passivation peak compared to COF@Zn and PVDF@COF@Zn. This indicates that ASEI not only
315 reduces dendrite formation and the Zn energy barrier but also decreases side reactions on the surface of the
316 Zn anode.

317 3.3 Optical cell testing

318



319

320 **Figure 8.** Optical photographs of PVDF@COF@Zn deposition/stripping as cross-sections at current
321 density 5 mA cm^{-2} at difference Zn anode.

322 To investigate the behavior of the protective layer, an in situ optical cell was set up to monitor the
323 Zn plating/stripping process (**Fig. S9**). A supplementary video further supports this observation, showing
324 the dynamic adaptation of the protective layer during the Zn deposition process. The cells used were

325 symmetric cells at a current density of 5 mA cm⁻². In Fig.8, the in-operando Zn plating/stripping process is
326 captured.

327 For the bare Zn, the first cycle shows smooth Zn deposits on the Zn anode. However, by the second
328 plating cycle, Zn deposition becomes non-uniform, as evident from a side view of the electrode. The
329 stripping style is uneven, leading to cluster areas and an inability to form a uniform layer. Moreover, when
330 the electrode surface is not smooth, subsequent plating cycles struggle to restore uniformity, resulting in Zn
331 dendrite formation on the Zn anode.

332 In contrast, During the initial Zn plating and stripping cycles, the COF layer effectively regulates
333 the uniform deposition of Zn. This means that in the first and second cycles, the COF layer remains intact
334 and maintains its structural integrity, allowing it to evenly distribute Zn ions across the surface. This
335 uniform distribution is critical as it prevents the formation of localized areas where Zn might accumulate
336 excessively, which could otherwise lead to dendritic growth. However, by the third cycle, the situation
337 changes. The repeated processes of Zn plating and stripping exert mechanical stress on the COF layer. This
338 stress, combined with the natural expansion and contraction of the Zn anode during cycling, can cause the
339 COF layer to develop microcracks. Once such cracks form, the layer loses its ability to evenly distribute Zn
340 ions across the surface. With the COF layer compromised, Zn begins to deposit unevenly during subsequent
341 plating. This uneven deposition creates localized areas with higher Zn concentrations, which are prone to
342 dendrite formation, eventually leading to a short circuit [49, 50]

343 The in-operando cell of PVDF@COF@Zn demonstrates that the protective layer adapts
344 dynamically to Zn volume changes, highlighting the mechanical flexibility and strength imparted by PVDF.
345 The incorporation of PVDF into the composite-ASEI provides essential mechanical support, allowing the
346 ASEI layer to absorb and distribute stress caused by Zn volume changes during plating/stripping cycles.
347 The PVDF matrix acts as a flexible support, maintaining structural integrity and preventing delamination
348 or cracking. Moreover, strong interfacial bonding between the COF and PVDF components, particularly
349 through interactions between the COF's carbonyl (C=O) groups and β-PVDF's positively charged carbon
350 atoms, ensures a stable composite structure. This bonding keeps the COF-PVDF films stable even under
351 significant volume changes, affirming that PVDF@COF as an ASEI is suitable for Zn-based battery
352 systems.

353

354

355

356 **Table. 1** Comparison of MOF/COF and PVDF-Composite as ASEI

ASEI materials	Method	Electrolytes	Current density	Areal Capacity	Voltages polarization	Life span	Ref.
BpTpCOF	Dip-coating	2M ZnSO ₄ + 0.2 M MnSO ₄	1 mA cm ⁻²	1 mAh cm ⁻²	~40 mV	>300 h	[40]
DAAQ-TFP COF	Dip-coating	2M ZnSO ₄	1 mA cm ⁻²	1 mAh cm ⁻²	~36 mV	>420 h	[34]
			2 mA cm ⁻²		~40 mV	>270 h	
TM-4F-COF	Doctor blading	2M ZnSO ₄	3 mA cm ⁻²	0.5 mAh cm ⁻²	~ 60.9 mV	>3000 h	[51]
ZIF-8	In situ growth	2M ZnSO ₄	0.5 mA cm ⁻²	0.2 mAh cm ⁻²	~70 mV	>680 h	[32]
ZIF-11	Doctor blading	2M ZnSO ₄	0.4 mA cm ⁻²	0.2 mAh cm ⁻²	-	>740 h	[33]
			0.5 mA cm ⁻²	0.2 mAh cm ⁻²	-	>620 h	
			1 mA cm ⁻²	0.5 mAh cm ⁻²	-	>555 h	
PVDF	Spin coating	2M ZnSO ₄	0.25 mA cm ⁻²	0.05 mAh cm ⁻²	~40 mV	>2000 h	[43]
TiO ₂ -PVDF	Drop cast	2M ZnSO ₄	0.885 mA cm ⁻²	0.885 mAh cm ⁻²	~50 mV	>2000 h	[52]
COF-PVDF	Transfer-Spin coating	2M ZnSO ₄	1 mA cm ⁻²	1 mAh cm ⁻²	~30 mV	>600 h	This work
				3 mAh cm ⁻²		>300 h	
				5 mAh cm ⁻²		>280 h	

357

358 The COF-PVDF as ASEI facilitates Zn²⁺ transport through a layer in which the ions are

359 guided by interactions with C=O and N-H functional groups within the COF structure. This allows

360 it to operate at high capacity, as shown in **Table 1**. The COF-PVDF can perform more than 600

361 cycles at a current density of 1 mA cm⁻² and a capacity of 1 mAh cm⁻², which is significantly

362 higher than the ~300 cycles achieved by BpTpCOF developed for dip-coating. Furthermore, the

363 voltage polarization of COF-PVDF is proved to be lower than that of BpTpCOF and other studies,

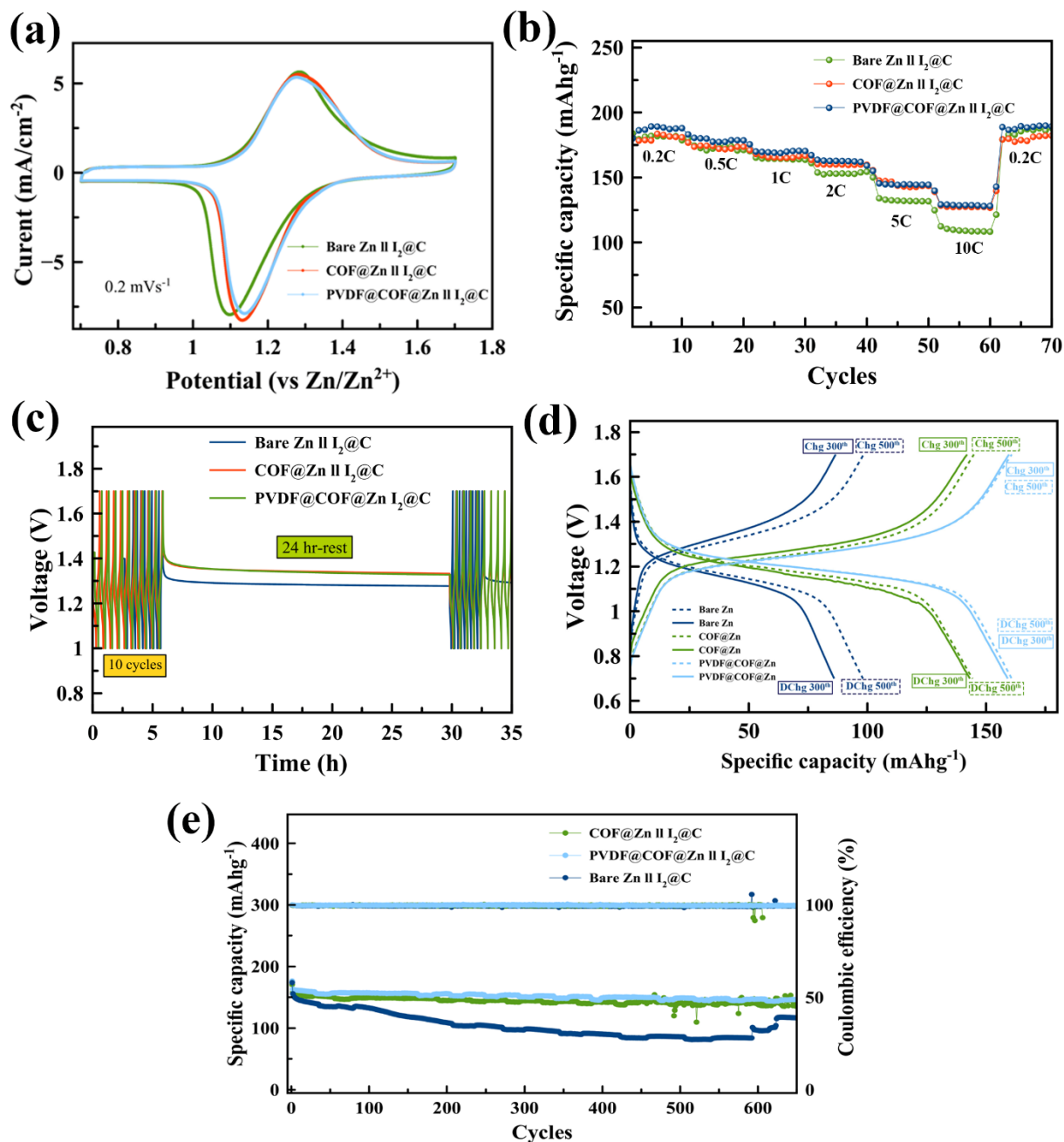
364 confirming that COF-PVDF enhances the performance of COF-based ASEI. Despite dramatic

365 volume changes during plating and stripping, ASEI adapts well. The COF-PVDF layer

366 dynamically adjusts during Zn deposition and reduces stress during Zn stripping, demonstrating

367 superior stability. Such superior features make the ASEI layer highly suitable for Zn-based

368 batteries.



372 **Figure 9.** Electrochemical performance of the bare Zn//I₂@C, COF@Zn//I₂@C, and
 373 PVDF@COF@Zn//I₂@C full cells: (a) CV profiles at 0.2 mV s⁻¹, (b) Rate capability at various current
 374 density, (c) Self-discharge performance of full cell, (d) Charge-discharge profiles at 300th and 500th cycles,
 375 and (e) Long-term cycling at current density of 3C.

376 To affirm the applicability of the ASEI layer for the aqueous battery systems, a full cell of Zn-
377 Iodine was used. In **Fig. 9a**, the CV curves for different anodes are shown. Both reduction and oxidation
378 exhibit similar redox peaks. However, the decrease in the difference between the oxidation and reduction
379 peaks of COF@Zn and PVDF@COF@Zn indicates that the electrochemical reactions are becoming more
380 reversible, suggesting faster kinetic reactions. This is related to the profile shown in Fig. 5C. Per se, the
381 modified ASEI not only improves the stability of the Zn anode but also facilitates overall reactions in the
382 full-cell batteries.

383 In **Fig. 9b**, the rate capability of COF@Zn and PVDF@COF@Zn reveals greater stability
384 compared to bare Zn. It is significant, therefore, that rate capability impacts not only the efficiency of the
385 Zn anode but also the overall performance of the full cell. Subsequently, after the cells underwent 10 cycles
386 and rested for 24 h, self-discharge measurements were conducted. Thus, the percentage of CE, reflecting
387 the batteries' charge retention efficiency, was computed for three anode materials: the bare Zn, COF@Zn,
388 and PVDF@COF. In **Fig. 9c**, it is noted that the CE of the post-rest period achieved 81.26% for the bare
389 Zn, 95.63% for COF@Zn, and 96.07% for PVDF@COF. These findings indicate that batteries with
390 COF@Zn and PVDF@COF anodes exhibit markedly superior charge retention compared to bare Zn
391 anodes, confirming that modifications of the anode can enhance battery performance. Furthermore, as
392 illustrated in **Fig. 9d**, there is a noticeable decline in specific capacity over cycles, particularly between the
393 300th and 500th cycles. However, PVDF@COF@Zn exhibits significantly greater stability compared to
394 COF@Zn and the bare Zn. Overall, PVDF@COF@Zn maintained its cycling performance for over 600
395 cycles, achieving a specific capacity of 160 mAh g⁻¹ and nearly 100% CE (**Fig. 9e**). These results validate
396 PVDF@COF as an effective ASEI for zinc-based battery systems.

397 **4. Conclusion**

398 In this work, a COF-PVDF composite as an ASEI for Zn-based batteries was successfully developed. The
399 interaction between COF and PVDF created a new ASEI surface that can operate under the high-volume
400 change of Zn deposition. The developed ASEI revealed promising chemical and mechanical properties,
401 allowing for uniform of Zn deposition even at high Zn volumes. The full-cell (Zn//I₂@C) results
402 demonstrated that samples with COF-PVDF showed much improved cyclability (>600 cycles at 3C) and
403 rate capability was in good agreement with the half-cell tests. Future research should focus on further
404 optimizing the chemical and mechanical properties of the ASEI layer and exploring its application in other
405 battery systems. Large-scale testing and real-world application studies will be essential to validate the
406 practical benefits of this technology in diverse energy storage scenarios.

407

408 **Acknowledgment**

409 We acknowledge the 90th Anniversary of Chulalongkorn University Scholarship, the Ratchadapisek
410 Sompote Fund, and The Program Management Unit for Human Resources and Institutional Development,
411 Research, and Innovation (B16F640166). V.A. thanks the Chulalongkorn Academic Advancement into its
412 2nd Century Project. Z.T. thanks the Royal Academy of Engineering in the UK. Synchrotron Light
413 Research Institute (Public Organization), Thailand is acknowledged for the provision of GIXRD beamtime
414 at Beamline 1.1W.

415

416 **Declaration of competing interest**

417 The authors declare that they have no known financial conflicts of interest or close personal ties that might
418 be perceived as having influenced the research presented in this paper.

419

420 **CRedit author statement**

421 Vipada Aupama: Conceptualization; Investigation; Formal analysis; Writing – original draft; Writing –
422 review & editing

423 Jinnawat Sangsawang: Investigation; Formal analysis; Writing – review & editing

424 Wathanyu Kao-ian: Formal analysis; Writing – review & editing

425 Suttipong Wannapaiboon: Formal analysis; Writing – review & editing

426 Jirapha Pimoei: Formal analysis; Writing – review & editing

427 Warunyoo Yoopensuk: Formal analysis; Writing – review & editing

428 Montree Opchoei: Formal analysis; Writing – review & editing

429 Zari Tehrani: Formal analysis; Writing – review & editing

430 Serena Margadonna: Formal analysis; Writing – review & editing

431 Soorathep Kheawhom: Conceptualization; Formal analysis; Funding; Supervision; Writing – review &
432 editing

434 **References**

- 435 1. Hoang Huy, V.P., L.T. Hieu, and J. Hur, *Zn metal anodes for Zn-ion batteries in mild aqueous electrolytes: Challenges and strategies*. *Nanomaterials*, 2021. **11**(10): p. 2746.
- 436 2. Jia, X., et al., *Active materials for aqueous zinc ion batteries: synthesis, crystal structure, morphology, and electrochemistry*. *Chemical Reviews*, 2020. **120**(15): p. 7795-7866.
- 437 3. Theerthagiri, J., et al., *Fundamentals and comprehensive insights on pulsed laser synthesis of advanced materials for diverse photo-and electrocatalytic applications*. *Light: Science & Applications*, 2022. **11**(1): p. 250.
- 438 4. Narthana, K., et al., *One-step synthesis of hierarchical structured nickel copper sulfide nanorods with improved electrochemical supercapacitor properties*. *International Journal of Energy Research*, 2021. **45**(7): p. 9983-9998.
- 439 5. Theerthagiri, J., et al., *Structural engineering of metal oxyhydroxide for electrochemical energy conversion and storage*. *Coordination Chemistry Reviews*, 2024. **513**: p. 215880.
- 440 6. Theerthagiri, J., et al., *Recent progress and emerging challenges of transition metal sulfides based composite electrodes for electrochemical supercapacitive energy storage*. *Ceramics international*, 2020. **46**(10): p. 14317-14345.
- 441 7. Theerthagiri, J., et al., *Recent progress on synthetic strategies and applications of transition metal phosphides in energy storage and conversion*. *Ceramics International*, 2021. **47**(4): p. 4404-4425.
- 442 8. Zheng, P., et al., *Powering battery sustainability: a review of the recent progress and evolving challenges in recycling lithium-ion batteries*. *Frontiers in Sustainable Resource Management*, 2023. **2**: p. 1127001.
- 443 9. Pakseresht, S., et al., *Recent Advances in All-Solid-State Lithium–Oxygen Batteries: Challenges, Strategies, Future*. *Batteries*, 2023. **9**(7): p. 380.
- 444 10. Wu, M., et al., *Fire-Safe Polymer Electrolyte Strategies for Lithium Batteries*. *Energy Storage Materials*, 2024: p. 103174.
- 445 11. Chitre, A., et al., *Towards a more sustainable lithium-ion battery future: recycling libs from electric vehicles*. *Batteries & Supercaps*, 2020. **3**(11): p. 1126-1136.
- 446 12. Duehnen, S., et al., *Toward green battery cells: Perspective on materials and technologies*. *Small Methods*, 2020. **4**(7): p. 2000039.
- 447 13. Thies, C., et al., *Assessment of social sustainability hotspots in the supply chain of lithium-ion batteries*. *Procedia CIRP*, 2019. **80**: p. 292-297.
- 448 14. Yang, J., et al., *Zinc anode for mild aqueous zinc-ion batteries: challenges, strategies, and perspectives*. *Nano-micro letters*, 2022. **14**: p. 1-47.
- 449 15. Shin, J., et al., *Aqueous zinc ion batteries: focus on zinc metal anodes*. *Chemical Science*, 2020. **11**(8): p. 2028-2044.
- 450 16. Kao-ian, W., et al., *Stability Enhancement of Zinc-Ion Batteries Using Non-Aqueous Electrolytes*. *Batteries & Supercaps*, 2022. **5**(5): p. e202100361.
- 451 17. Zhang, X., et al., *Design Strategies for Aqueous Zinc Metal Batteries with High Zinc Utilization: From Metal Anodes to Anode-Free Structures*. *Nano-Micro Letters*, 2024. **16**(1): p. 75.
- 452 18. Hoang Huy, V., L. Hieu, and J. Hur, *Zn metal anodes for Zn-ion batteries in mild aqueous electrolytes: challenges and strategies*. *Nanomaterials (Basel)* **11**, 2746. 2021.
- 453 19. Wang, T., et al., *Anode Materials for Aqueous Zinc Ion Batteries: Mechanisms, Properties, and Perspectives*. *ACS Nano*, 2020. **14**(12): p. 16321-16347.
- 454 20. Wang, X., et al., *Solid electrolyte interface in Zn-based battery systems*. *Nano-Micro Lett.* **14** (1), 205 (2022).
- 455 21. Xiong, P., et al., *Recent progress of artificial interfacial layers in aqueous Zn metal batteries*. *EnergyChem*, 2022. **4**(4): p. 100076.
- 456 22. Du, W., et al., *Challenges in the material and structural design of zinc anode towards high-performance aqueous zinc-ion batteries*. *Energy & Environmental Science*, 2020. **13**(10): p. 3330-3360.

- 481 23. Yang, Y., et al., *Redistributing Zn-ion flux by interlayer ion channels in Mg-Al layered double hydroxide-based*
482 *artificial solid electrolyte interface for ultra-stable and dendrite-free Zn metal anodes*. Energy Storage
483 Materials, 2021. **41**: p. 230-239.
- 484 24. Gopalakrishnan, M., et al., *Metal-organic framework/mxene heterostructure and its derivatives as electrode*
485 *materials for rechargeable Zn-based batteries: Design strategies and perspectives*. Chemical Engineering
486 Journal, 2024: p. 149624.
- 487 25. Cui, J., et al., *Confinement of zinc salt in ultrathin heterogeneous film to stabilize zinc metal anode*. Small,
488 2021. **17**(28): p. 2100722.
- 489 26. Panda, S., et al., *MXene based emerging materials for supercapacitor applications: Recent advances,*
490 *challenges, and future perspectives*. Coordination Chemistry Reviews, 2022. **462**: p. 214518.
- 491 27. Lee, S.J., et al., *Heteroatom-doped graphene-based materials for sustainable energy applications: A review*.
492 Renewable and Sustainable Energy Reviews, 2021. **143**: p. 110849.
- 493 28. Zhao, Z., et al., *Long-life and deeply rechargeable aqueous Zn anodes enabled by a multifunctional*
494 *28brightener-inspired interphase*. Energy & Environmental Science, 2019. **12**(6): p. 1938-1949.
- 495 29. Chen, P., et al., *An artificial polyacrylonitrile coating layer confining zinc dendrite growth for highly reversible*
496 *aqueous zinc-based batteries*. Advanced Science, 2021. **8**(11): p. 2100309.
- 497 30. Hao, J., et al., *Designing dendrite-free zinc anodes for advanced aqueous zinc batteries*. Advanced Functional
498 Materials, 2020. **30**(30): p. 2001263.
- 499 31. Yang, H., et al., *Constructing a super-saturated electrolyte front surface for stable rechargeable aqueous*
500 *zinc batteries*. Angewandte Chemie, 2020. **132**(24): p. 9463-9467.
- 501 32. Cui, M., et al., *In-situ grown porous protective layers with high binding strength for stable Zn anodes*.
502 Chemical Engineering Journal, 2022. **434**: p. 134688.
- 503 33. He, M., et al., *Suppressing dendrite growth and side reactions on Zn metal anode via guiding interfacial*
504 *anion/cation/H₂O distribution by artificial multi-functional interface layer*. Energy Storage Materials, 2022.
505 **44**: p. 452-460.
- 506 34. Park, J.H., et al., *Self-assembling films of covalent organic frameworks enable long-term, efficient cycling of*
507 *zinc-ion batteries*. Advanced Materials, 2021. **33**(34): p. 2101726.
- 508 35. Geng, K., et al., *Covalent organic frameworks: design, synthesis, and functions*. Chemical reviews, 2020.
509 **120**(16): p. 8814-8933.
- 510 36. Li, J., et al., *Bulk COFs and COF nanosheets for electrochemical energy storage and conversion*. Chemical
511 Society Reviews, 2020. **49**(11): p. 3565-3604.
- 512 37. Zhao, J., et al., *Covalent organic framework film protected zinc anode for highly stable rechargeable aqueous*
513 *zinc-ion batteries*. Energy Storage Materials, 2022. **48**: p. 82-89.
- 514 38. Zhao, Z., et al., *Horizontally arranged zinc platelet electrodeposits modulated by fluorinated covalent*
515 *organic framework film for high-rate and durable aqueous zinc ion batteries*. Nature communications, 2021.
516 **12**(1): p. 6606.
- 517 39. Khayum, A., et al., *Zinc ion interactions in a two-dimensional covalent organic framework based aqueous*
518 *zinc ion battery*. Chemical science, 2019. **10**(38): p. 8889-8894.
- 519 40. Aupama, V., et al., *Stabilizing a zinc anode via a tunable covalent organic framework-based solid electrolyte*
520 *interphase*. Nanoscale, 2023. **15**(20): p. 9003-9013.
- 521 41. Guo, Z., et al., *A dynamic and self-adapting interface coating for stable Zn-metal anodes*. Advanced
522 Materials, 2022. **34**(2): p. 2105133.
- 523 42. Ruan, L., et al., *Properties and applications of the β phase poly(vinylidene fluoride)*. Polymers, 2018. **10**(3):
524 p. 228.
- 525 43. Hieu, L.T., et al., *Zn anode with flexible β -PVDF coating for aqueous Zn-ion batteries with long cycle life*.
526 Chemical Engineering Journal, 2021. **411**: p. 128584.
- 527 44. Park, H., R.K. Bera, and R. Ryoo, *Microporous 3D graphene-like carbon as iodine host for zinc-based battery–*
528 *supercapacitor hybrid energy storage with ultrahigh energy and power densities*. Advanced Energy and
529 Sustainability Research, 2021. **2**(10): p. 2100076.
- 530 45. Li, W., K. Wang, and K. Jiang, *A high energy efficiency and long life aqueous Zn–I₂ battery*. Journal of
531 materials chemistry A, 2020. **8**(7): p. 3785-3794.
- 532 46. Polat, K., *Energy harvesting from a thin polymeric film based on PVDF-HFP and PMMA blend*. Applied Physics
533 A, 2020. **126**: p. 1-8.

- 534 47. Tang, Y., et al., *A π - π Stacked High-Performance Organic Anode for Durable Rocking-Chair Zinc-Ion Battery*.
535 Batteries, 2023. **9**(6): p. 318.
- 536 48. Chen, T., M. Li, and J. Liu, *π - π stacking interaction: a nondestructive and facile means in material*
537 *engineering for bioapplications*. Crystal Growth & Design, 2018. **18**(5): p. 2765-2783.
- 538 49. Wang, T., et al., *Planar and dendrite-free zinc deposition enabled by exposed crystal plane optimization of*
539 *zinc anode*. Energy Storage Materials, 2022. **53**: p. 273-304.
- 540 50. Cao, P., et al., *Manipulating uniform nucleation to achieve dendrite-free Zn anodes for aqueous Zn-ion*
541 *batteries*. ACS Applied Materials & Interfaces, 2021. **13**(41): p. 48855-48864.
- 542 51. Wang, Y., et al., *Interface Regulation by Fluorinated Vinylene-Linked Covalent Organic Framework for Highly*
543 *Stable Zn Anode*. Journal of Materials Chemistry A, 2024.
- 544 52. Zhao, R., et al., *Redirected Zn electrodeposition by an anti-corrosion elastic constraint for highly reversible*
545 *Zn anodes*. Advanced Functional Materials, 2021. **31**(2): p. 2001867.

546

547